Integrated Flow and Stress Modeling for Infusion and Curing Process in Liquid Composite Molding

KALYAN SHRESTHA[1], RYAN ENOS[2], XUXIAO LI[1], QINGXUAN WEI[2], MUTHU ELENCHEZHIAN[2], DIANYUN ZHANG[2,*] and JIM LUA[1,*]

ABSTRACT

Liquid composite molding, such as resin transfer molding and vacuum-assisted resin transfer molding, is an economical composite manufacturing technique for large-scale parts. Modeling of the flow phenomena during the infusion process and the stress build-up in the subsequent curing process is imperative to improve part quality and reduce the number of trial tests. Despite the abundance of literature in both flow and stress modeling, an integrated model that couples the flow and stress physics is lacking. In this work, we combined the state-of-the-art flow and stress models to establish such an integrated framework. An infusion flow model is developed with the commercial computational fluid dynamics software STAR-CCM+, which incorporates the submodels to account for flow front evolution, compaction, and resin reaction. Several stress-based models are implemented in ABAQUS to account for fabric draping, compaction, and curing-induced thermal and chemical deformation. To demonstrate the importance of modeling the coupled physics, we conducted three case studies to show (1) effects of draping on the flow front evolution, (2) effects of degree of cure advection during infusion on the curing-induced stress build-up, and (3) effects of flow-compaction coupling on the flow front and dry spot formation in vacuum infusion.

Key Words: Liquid composite molding, Infusion, Curing.

[1]Global Engineering and Materials, Inc., 1 Airport Place, Suite 5 & 6, Princeton, NJ 08540, USA.
[2]School of Aeronautics and Astronautics, Purdue University, 701 W Stadium Ave, West Lafayette, IN 47907-2045, USA.
*Corresponding Author(s)
Jim Lua – jlua@gem-innovation.com
Dianyun Zhang– dianyun@purdue.edu

INTRODUCTION

The liquid composite molding (LCM) process can be divided into two stages. In the infusion state, the resin in the liquid state is first impregnated into a fabric material. In the subsequent curing stage, the resin is exposed to an elevated temperature to solidify (referred to as gelation) and bond together with the fabric to form the composite. Multiphysics modeling and simulation have been applied to study the infusion and curing so that the trial-and-error cost can be reduced to minimize porosities, process time, and residual stress/strain. There are two main "forks" in the existing process simulation literature: the flow-based "fluid mechanics" models that focus on the pre-gelation resin flow, and the stress-based "solid mechanics" models that focus on the post-gelation stress build-up and deformation. It has been shown that flow-based models successfully predict the resin flow front evolution [1], dry spot (unfilled region) formation [2], and microscale porosities [3]. The stress-based models have shown capabilities in predicting the warpage, spring-in, and compaction for a variety of geometries [4–6]. However, the flow-based and stress-based models typically have their own problem set, and the coupling between the two simulations is lacking. As the understanding and expectation of composite manufacturing increase, there is a need to consider the more complex interaction between the fluid and solid mechanics in LCM processes.

In this work, we leveraged the state-of-the-art flow-based and stress-based models and established a framework for information exchange between the two models. The commercial computational fluid dynamics (CFD) software STAR-CCM+ is employed to model the flow behavior, and the commercial finite element analysis (FEA) software ABAQUS is employed to predict the stress and strain field. Then, the user-defined subroutines are implemented in both software to enable the mapping of arbitrary variables between the two models in real-time simulation runs. With such capability, we conducted three case studies to demonstrate the importance of coupling between the flow-based and stress-based models for prediction accuracy.

In the first case study, the effect of fabric draping [7] on the flow front prediction is investigated. The fabric shear angle is predicted from the ABAQUS model and mapped into the STAR-CCM+ model to enable anisotropic flow front predictions. In the second case study, the degree of cure (DOC) evolution during the infusion process is tracked in STAR-CCM+ via the passive scalar tracking technique. The DOC is then fed into ABAQUS as an initial condition to predict the curing-induced residual stress/strain. The purpose of this study is to investigate the effect of initial DOC on the cure-induced deformation response, as most of the existing models assume uniformly zero DOC as the initial condition. In the third case study, the flow-compaction coupling [8] in the vacuum infusion process is studied. The fabric compaction is computed in ABAQUS to update the compaction-dependent permeability and porosity in STAR-CCM+.

MODEL DESCRIPTION

The flow-based and stress-based models adopted in this work have been described in detail in the previous publications [4,9,10]. Here, we will focus on the coupling mechanism between the two models and only give brief descriptions of the ABAQUS and STAR-CCM+ implementation when necessary.

Information Exchange between ABAQUS and STAR-CCM+

We implemented a general framework to map the variable set V from STAR-CCM+ to ABAQUS and the variable set W from ABAQUS to STAR-CCM+, as shown in Figure 1. The STAR-CCM+ user code (in C++) is implemented to extract the mesh coordinates and the variable set V. The ABAQUS Python script is employed to extract the mesh coordinates and the variable set W. A highly-efficient KD-tree interpolation algorithm [11] is adopted to map arbitrary variables between the two sets of meshes. Finally, the ABAQUS UMAT is used to read the external variable set V to define the material constitutive behaviors.

Draping Model

The material draping is modeled as a hyperelastic material behavior which is implemented in the ABAQUS VUMAT subroutine. The predicted shear strain in-plane component γ_{12} is mapped into STAR-CCM+. The permeability K and porosity ε are then calculated as functions of γ_{12}. Here, we investigate both a theoretical-based and a statistical-based approach to correlate K and γ_{12}.

The theoretical-based approach is based on the description of a unit cell in non-crimped textile (Figure 2) [12][12]. In a unit cell, the fiber tows are of lengths a and b and the radius is r.

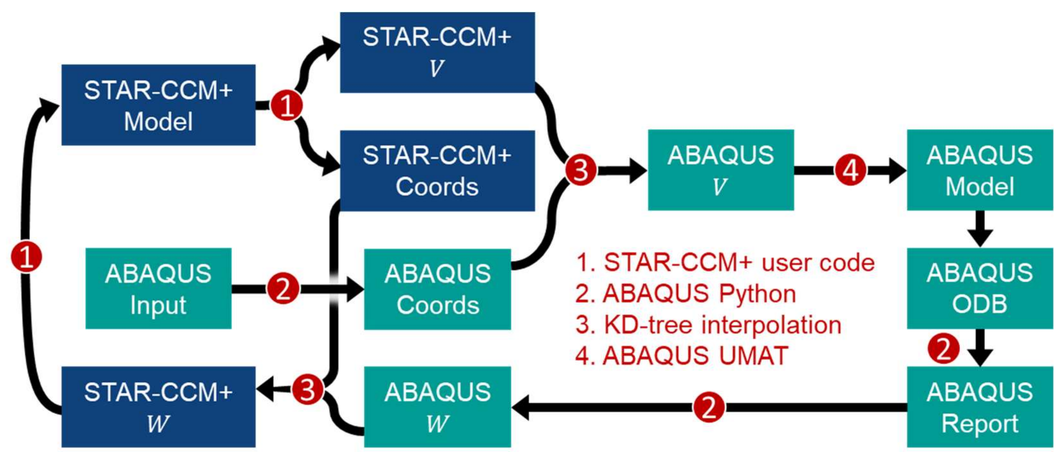

Figure 1. Information exchange framework between ABAQUS and STAR-CCM+.

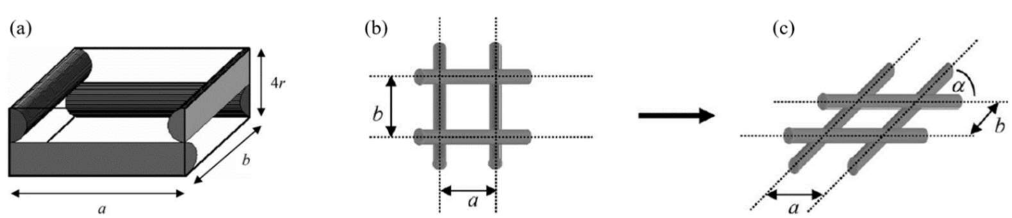

Figure 2. (a) Schematic of a unit cell of a woven composite fabric. (b) Two-dimensional view of the undeformed fabric with fiber tow axes a and b. (c) Deformed fabric due to scissor drape. Adapted from [12].

The theoretical-based approach considers the so-called "scissor drape" where the unit cell volume V changes while the fiber volume fraction V_f remains constant. The porosity and permeability of the deformed textile can be calculated as Eqs. (1) and **Error! Reference source not found.**:

$$\varepsilon_{def} = \varepsilon \left(\frac{4ab - \dfrac{\pi r(a+b)(1-\varepsilon_{min})}{\sin \gamma}}{4ab - \pi r(a+b)(1-\varepsilon_{min})} \right) \tag{1}$$

$$k_{def} = k \left(\frac{4ab - \dfrac{\pi r(a+b)(1-\varepsilon_{min})}{\gamma}}{4ab - \pi r(a+b)(1-\varepsilon_{min})} \right)^3 \sin^2 \gamma \tag{2}$$

Here, k is the undeformed permeability, $\varepsilon_{min} = 0.09$ is a theoretical minimum residual inter-filament porosity. a, b, and r can be obtained from micrographic measurements. The infusion process in a draped material is known to exhibit anisotropic permeability, whose permeability principal values can be estimated as Eqs. (3) and **Error! Reference source not found.**:

$$K_1 = k_{def} \sqrt{\frac{1+\cos\gamma}{1-\cos\gamma}} \tag{3}$$

$$K_2 = k_{def} \sqrt{\frac{1-\cos\gamma}{1+\cos\gamma}} \tag{4}$$

The statistical-based approach is based on [7]. The authors conducted a large set of permeability characterization experiments using woven carbon fiber and olive oil as the infusion fluid, and varied shear angles between 0° to 40°. Then, the curve was fitted on the experimental data to obtain an empirical formulation of the deformation-dependent permeabilities and porosity, as listed by Eqs. (5) – (7).

$$K_1 = (-6.641\,\gamma^4 + 13.28\,\gamma^3 - 8.414\,\gamma^2 + 2.4\,\gamma + 0.6028) \times\ 10^{-10} \tag{5}$$

$$K_2 = \ (-7.7\,\gamma^4 + 14.66\,\gamma^3 - 9.261\,\gamma^2 + 1.605\,\gamma + 0.5313) \times\ 10^{-10} \tag{6}$$

$$\varepsilon = 1 - \frac{1-\varepsilon_0}{\cos\gamma} \tag{7}$$

where ε_0 is the undeformed porosity. The unit of shear angle is radius, and the unit of permeability is m^2.

DOC Transport Model

The DOC is evolved over time under a constant infusion temperature. In this work, we use the Epon862/W resin system with an infusion temperature of 121°C. The evolution of the DOC is tracked using the methodology in [13], which is written as Eq. (8):

$$\frac{\partial \phi}{\partial t} + v \cdot \nabla \phi = R_c(\phi, T) \tag{8}$$

Here ϕ is the DOC, v is the resin flow velocity, and R_c is the chemical reaction rate as a function of ϕ and temperature T. R_c is defined by a mixed order autocatalytic model, which is written as Eq. (9):

$$R_c = (a_1(T) + a_2(T)\phi^m)(1-\phi)^n \tag{9}$$

where a_1 and a_2 take the form $a_i = A_i \exp(-\Delta E_i/RT)$ [14]. The phenomenological values of the parameters A_1, ΔE_1, A_2, ΔE_2, m, and n used in our infusion-curing simulation are 42.7, 47800, 17800, 48300, 0.865, and 1.28, respectively. In STAR-CCM+ simulation, DOC is implemented as a passive scalar advection model, and the changes in the DOC- and temperature-dependent viscosity (μ) are computed as Eq. (10):

$$\mu = \mu_\infty \exp\left(\frac{U}{RT} + k_1\phi + k_2\phi^2\right) \tag{10}$$

where the values of the parameters μ_∞, U, k_1, and k_2 are 7.7×10^{-5}, 2.52×10^{2}, 4.47, and 13.58, respectively [14].

After the infusion simulation in STAR-CCM+, the DOC field is mapped into a viscoelastic ABAQUS model to simulate the curing process and residual stress. The curing temperature is 177°C. Details of the ABAQUS model are referred to [9]

Flow-Compaction Model

The flow-compaction model has been detailed in a previous publication [9]. The modeling strategy is briefly summarized as follows. The infusion flow is predicted by STAR-CCM+ and the compaction during the vacuum infusion is predicted by ABAQUS. In the STAR-CCM+ model, the permeability is a function of porosity according to the Carman-Kozeny equation. The porosity is informed based on the volumetric strain computed by the ABAQUS model. In the ABAQUS model, the fabric is considered as a linear elastic material inspired by [15]. The resin pressure mapped from the STAR-CCM+ model partially balances the compaction stress according to Terzaghi's principle.

RESULT AND DISCUSION

Case Study 1: Coupling of Draping and Resin Flow

The setup of the draping simulation in ABAQUS is shown in **Error! Reference source not found.**. The blank holder and die support are 0.25 mm (the thickness of the fabric) apart in the Z direction and they were created as one part (referred to as the BHDS) to mimic the situation that the blank holder was combined with the die support by translucent tapes in the real experiment. Initially, the blank holder contacts the upper surface of the fabric and the die support were in contact with the lower one without compression. The BHDS together with punch was created as a rigid body, and it was fixed during the whole process. A quarter of the fabric was included in the model (150×150 mm) with symmetric boundary conditions along the bottom edge (where Y = 0) and the left edge (where X = 0). A nonuniform mesh was generated for the fabric. The mesh size was 6.25 mm at the four corners, while the mesh size at the inner region was refined to 2.94 mm. Contact pairs were identified between surfaces that can touch, and the penalty friction method was used to model the tangential interaction behavior at the tool-fabric and fabric-fabric interfaces with the friction coefficient set to 0.3. The fabric was first draped along the -Z direction for 65 mm in 1 minute with constant speed. Then, all the parts are held still for 5 minutes for relaxation.

Output from the ABAQUS model containing the shearing angle data was imported to STAR-CCM+, as shown in Figure 4. The model utilizes symmetric boundary conditions at the edges adjacent to the resin inlet gate (Figure 4(b)). The resin is injected from the pole of the hemisphere and the vacuum vent is at the boundary of the fabric, corresponding to the two edges forming the bottom right corner of the domain. Contrary to the ABAQUS mesh, the meshing strategy in the STAR-CCM+ model refines the inlet, symmetry, edges, and outlet to avoid meshing singularities. In the infusion simulations, the resin density and dynamic viscosity are $\rho = 970$ kg/m^3 $\mu = 0.1$ Pa · s, respectively, and the reference porosity and permeability of the undeformed fabric are $\varepsilon = 0.6$ and $k = 3 \times 10^{-11}$ m^2, respectively.

Draping results in local deformities in the woven fabric, which is illustrated by the contours of resultant shear angles between warp and weft tows in Figure 4. The maximum fabric deformation is near the base of the hemisphere. The corresponding porosity and permeability are shown in Figure 5. Porosity is minimally affected by draping in the theoretical-based approach (Figure 5(a)).

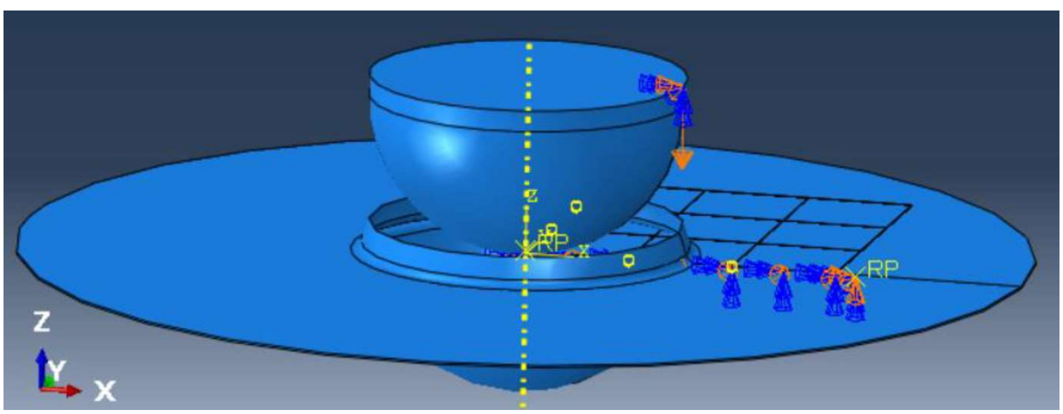

Figure 3. Hemisphere draping model in ABAQUS.

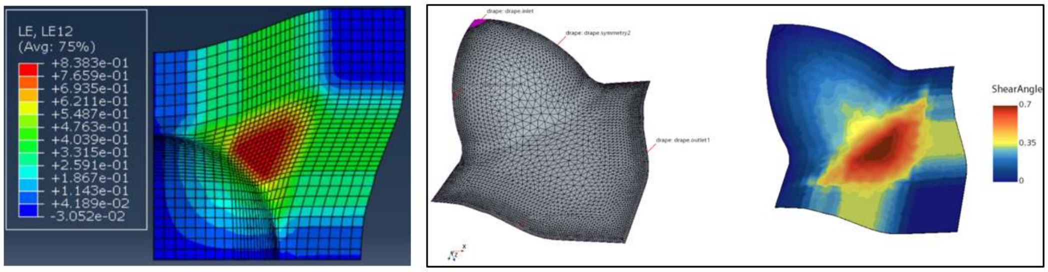

(a) (b)

Figure 4. (a) ABAQUS shear angle and mesh. (b) STAR-CCM+ mesh and mapped shear angle.

As discussed earlier, the scissor drape does not cause significant spatial variation in the fiber volume fraction, and thus the porosity of the deformed fabric does not experience significant impact in the region of deformation. The statistical-based approach is not built on the assumptions that "fiber volume fraction remains same after deformation" but is based, rather, on empirical fit from a large dataset, and thus the spatial variations of the fiber volume fraction are considerable (Figure 5(c)).

The effect of draping models on the infusion process is evaluated by comparing the progression of the simulated flow front (Figure 4). High shear deformation corresponds to higher K_1/K_2 ratio and faster flow in the K_1 permeability direction. This can be observed distinctly in Figure 6 (d, f, g), where the flow front accelerates in the K_1 permeability direction. This highlights the effect of draping on flow behavior. Moreover, the statistical- and theoretical-based approaches show some differences in the filling time. The statistical-based approach has predicted a shorter filling time because the porosity is significantly reduced in the shear deformation zone (see Figure 5(c)) compared to the theoretical-based approach.

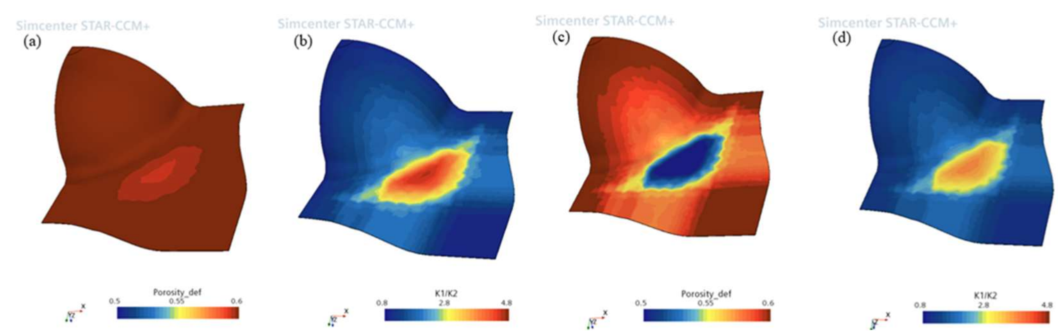

Figure 5. Comparison of contour maps obtained from theoretical-based approach ((a) & (b)) and statistical-based approach ((c) & (d)). (a) and (c) shows the porosity. (b) and (d) shows the permeability ratio K_1/K_2.

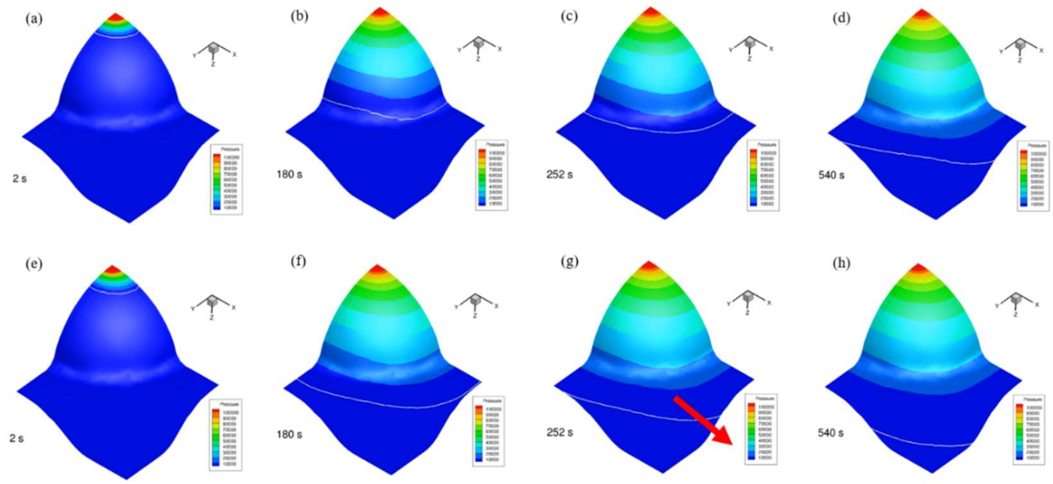

Figure 6. Evolution of the flow front (indicated by solid white line) and pressure distribution contour map in an infusion simulation of a hemisphere draping model plotted at increasing physical timesteps; (a, b, c, d) theoretical-based approach, and (e, f, g, h) statistical-based approach. Red arrow denotes K_1 permeability direction.

Case Study 2: Coupling of Infusion and Curing

In this study, we simulate the infusion process for an L-shaped beam. The L-shape is made from 6-by-6 inch fabric plies with outer corner radius of 0.75 inches and thickness of 0.125 inches. As shown in Figure 7, the resin is injected from the upper left corner and vented from the lower right corner of the L beam. The DOC is tracked as the resin infusion (temperature held at 120°C). It can be seen in Figure 7 that the DOC is the highest at the flow front and negligible at the inlet. This is because the resin at the flow front spends a comparatively longer time in the computational domain, and thus, the DOC is the highest. At the inlet, the resin held at room temperature is continuously injected and thus the DOC is negligible. Also, the viscosity of the resin near the flow front keeps increasing over time, which augments deceleration of the flow front progression. After the infusion-curing process, the part is allowed some time to bleed the excess resin. When the continuous resin injection and resin bleeding balance with each other, a quasi-stationary state of the DOC is established, which sets the initial condition of DOC for the second stage.

The STAR-CCM+ CFD infusion simulation results in a distribution of DOC. Since gelation has not occurred yet, any stress development is able to relax. The capability to use the DOC at the end of the infusion simulation as the initial condition in the FEA curing model has been developed. The user-subroutines UEXTERNALDB and UMAT are coordinated to define the DOC at the integration points in ABAQUS.

Typically, a homogeneous uniformly zero or small initial DOC is assumed in the curing analysis, and Figure 8 (a) shows the cure progression and deformation response of an example L-beam composite part (case A). Figure 8 (b) shows the cure progression and deformation response when the infusion analysis is used to define the initial condition for the curing analysis (case B). In this example, the composite structure is modeled as a free part and hence the internal stress response is manifested as deformation which can be seen observed directly. It can be seen that gelation occurs earlier in case B, as deformation begins at this point when the stress due to chemical shrinkage is no longer able to relax. Deformation begins at the outlet end and propagates towards the inlet as the entire part becomes gelled, and the two deformation results nearly converge by the end of the analysis. Figure 9 presents a plot of the spring-in angle versus time for case A, which is uniform along the length, and plotted for case B separately near the inlet and the outlet.

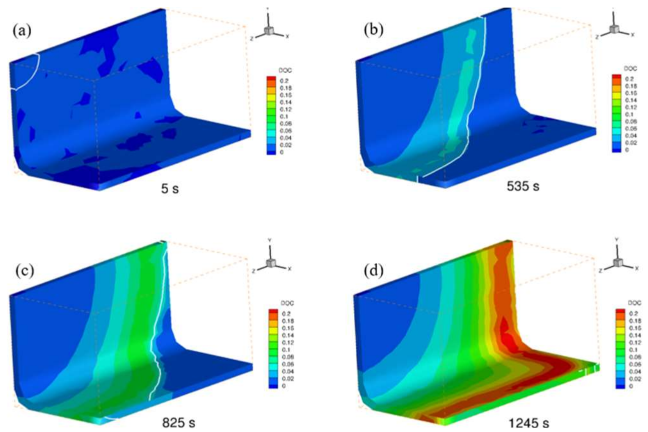

Figure 7. Infusion-curing coupling simulation for an L-beam. Color is DOC and white is flow front.

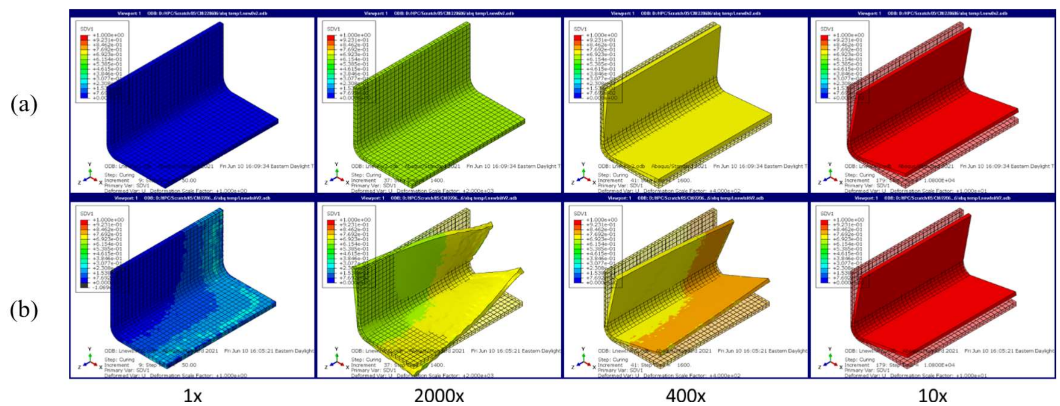

Figure 8. Cure history and deformation response of example L beam; (a) initial uniformly zero DOC case, and (b) the mapped initial condition case.

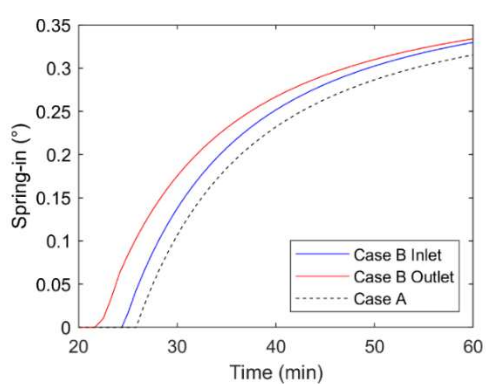

Figure 9. Spring-in response of example L beam analyses corresponding to initial uniformly zero DOC and the mapped initial condition near the inlet and outlet.

Case Study 3: Coupling of Flow and Compaction in Vacuum Infusion

In this study, we applied the flow-compaction model to study the vacuum infusion process for the previously described L-shaped beam. The strain along the out-of-plane direction for the dry fabric under 1 atm compaction is shown in Figure 10. It can be seen that the thickness of the fabric decreases at the L-edges (green box), while the thickness slightly increases at the L-corner (red box). Such thickness increase in the corner is commonly observed in the autoclave molding literature [16,17], which is attributed to the difficulty in deformation due to shear modulus. Given the difference between the autoclave and infusion processes, the simulation corner thickness variation here is subject to future investigation (e.g., conduct micrographic analysis on the cross section to examine the thickness variation). Compaction leads to fabric deformation that further leads to changes in permeability. Because the thickness increases in the L-corner, the fiber volume fraction (V_f) decreases, and the permeability (K) increases. As such, the flow front accelerates in the corner region as seen in Figure 11. In the simulation described in Figure 6, the resin is injected from the upper left corner and vent from the lower right corner. Due to the flow acceleration in the corner, residual air is trapped at the upper right corner by the end of the infusion. This is also observed in the experiment, where the trapped air in the upper right corner eventually leads to a dry spot.

A set of infusion experiments were conducted for the L-beam infusion with different resin system (Epon862/W and silicon oil), fabric layout configuration (with and without peel ply), and inlet/outlet port design. Figure 12 summarizes three typical flow front behaviors. Among the infusion experiments that we conducted, the majority of the flow front behaviors fall into the mild flow acceleration and the severe flow acceleration case. A mild flow acceleration can be considered a result of thickness increase due to compaction (Figure 11) but a severe acceleration should be the consequence of the race tracking phenomenon, where an air channel is created between the fabric and mold wall (or between the vacuum and the fabric).

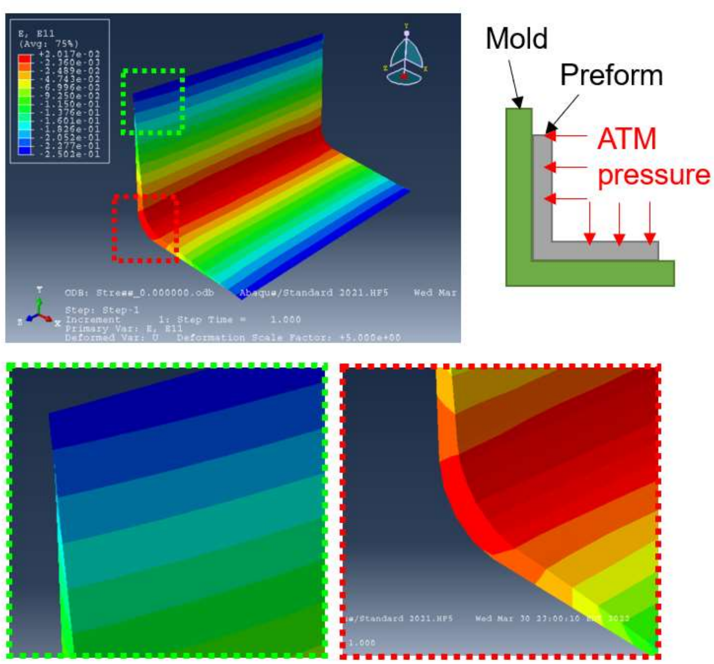

Figure 10. Compaction of dry fiber of the L-beam.

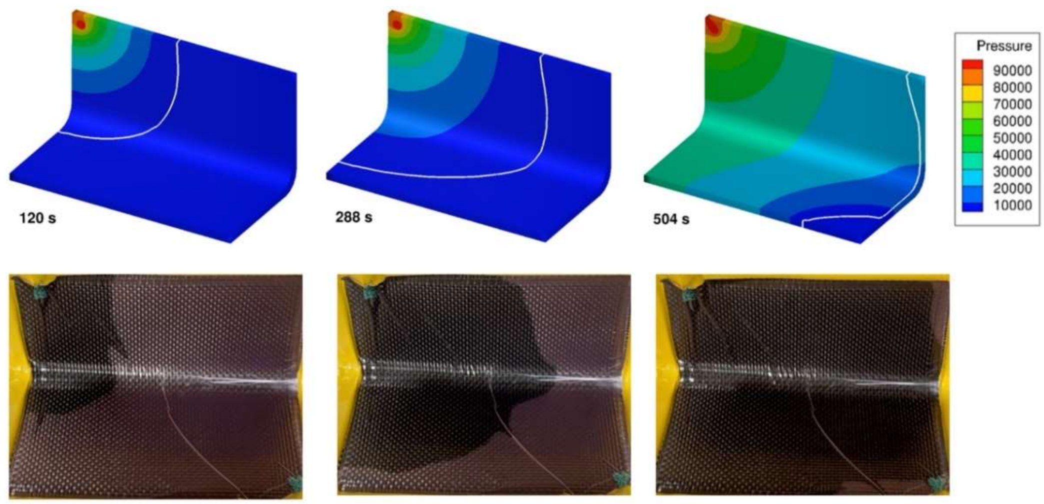

Figure 11. L-beam infusion simulation with flow compaction coupling. Flow front at the L-corner accelerates in the simulation due to the thickness increase. Flow front acceleration is commonly observed in experiments.

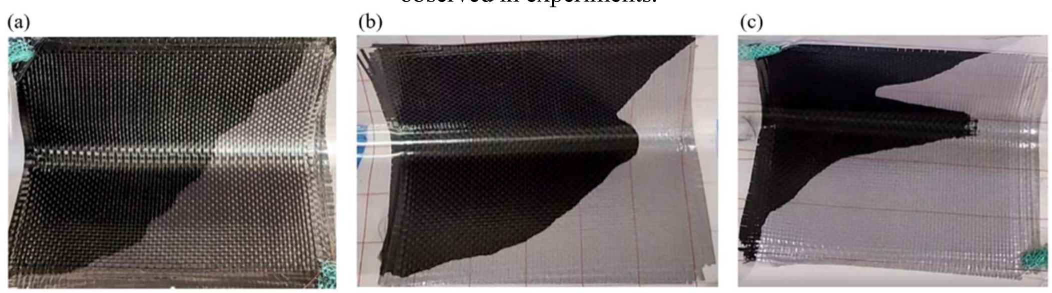

Figure 12. Typical flow front behaviors of L-beam infusion (a) No flow acceleration (b) Mild flow acceleration (c) Severe flow acceleration.

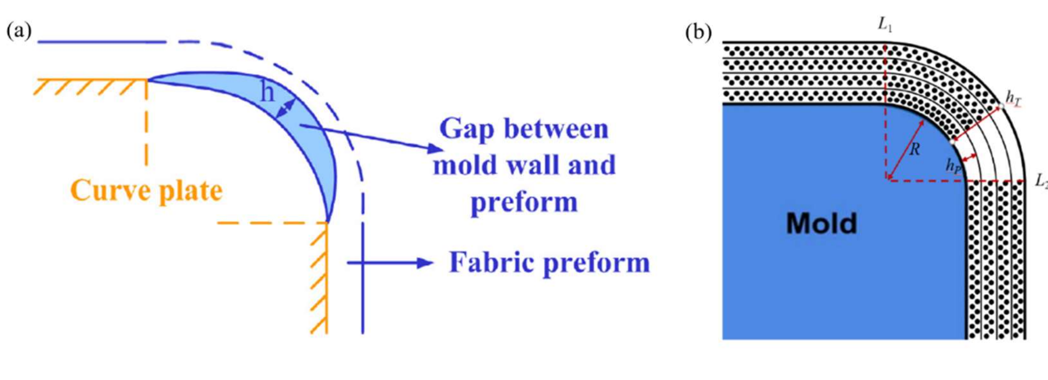

Figure 13. (a) Air channel between the mold wall and preform (b) Increase in V_f due to in-plane squeezing of the fiber.

Race tracking at the corner of composite structure during the infusion has been reported in the literature [18], as shown in **Error! Reference source not found.**(a). Given the nature of flow acceleration that occurs abruptly, we hypothesize that race tracking is the dominant mechanism over the effects of flow-compaction coupling. In the literature, flow deceleration at the bend region is also reported, which is attributed to the in-plane squeezing of the fiber [19]. It is hypothesized that the fabric V_f at the outer radius remains constant in a curved surface, whereas V_f at the inner radius increases (**Error! Reference source not found.**(b)). As a result, permeability decreases at the corner region and the flow slows down.

We summarize that there are counteracting factors for the variability of permeability K at the curved/corner region of a structure: (1) race tracking effect; (2) in-plane squeezing and/or stretching of fiber; (3) out-of-plane thickness variation. Based on our study, race tracking is hypothesized to be the dominating factor. However, the air channels that cause race tracking can be eliminated after considerable improvements to the process. Eventually, the in-plane fabric deformation competes with the out-of-plane deformation. The in-plane squeezing tends to increase V_f and decrease K, while the corner thickness increase tends to decrease V_f and increase K.

CONCLUSIONS

In this work, we demonstrated the capability of coupling the state-of-the-art flow-based and stress-based models of LCM processes. A general information exchange framework is established to communicate between the flow model implemented in STAR-CCM+ and the stress model implemented in ABAQUS. Three case studies are conducted to show the importance of capturing the coupled physics between the fluid mechanics and solid mechanics in LCM. The results are summarized as follows:

- In the draping study, the shear angle due to the drape is found to cause anisotropy and irregular flow front in the infusion
- In the infusion-curing coupling study, the initial DOC field developed in the infusion process is found to cause a nonuniform stress response history during the curing process of an L-shaped beam. However, the initial DOC field has negligible influence on the final spring-in angle.
- In the flow-compaction coupling study, it is found that the flow accelerates at the L corner region, which is attributed to both race tracking and the permeability variation due to compaction.

Future work includes conducting experiments to validate the effects of initial DOC and conducting micrographic analysis to determine the deformation at the L corner region. The ABAQUS and STAR-CCM+ models will also be further enhanced to include advanced features such as heat transfer analysis for the infusion simulation and stress relaxation for the compaction simulation.

REFERENCES

1. Šimáček P, Advani SG. Desirable features in mold filling simulations for Liquid Composite Molding processes. Polymer Composites 2004;25:355–67. https://doi.org/10.1002/PC.20029.
2. Matsuzaki R, Kobayashi S, Todoroki A, Mizutani Y. Flow control by progressive forecasting using numerical simulation during vacuum-assisted resin transfer molding. Composites Part A: Applied Science and Manufacturing 2013;45:79–87. https://doi.org/10.1016/J.COMPOSITESA.2012.09.014.

3. Devalve C, Pitchumani R. Simulation of void formation in liquid composite molding processes. Composites Part A: Applied Science and Manufacturing 2013;51:22–32. https://doi.org/10.1016/J.COMPOSITESA.2013.03.016.
4. Chen W, Zhang D. Improved prediction of residual stress induced warpage in thermoset composites using a multiscale thermo-viscoelastic processing model. Composites Part A: Applied Science and Manufacturing 2019;126:105575. https://doi.org/10.1016/J.COMPOSITESA.2019.105575.
5. Johnston A, Vaziri R, Poursartip A. A Plane Strain Model for Process-Induced Deformation of Laminated Composite Structures: Http://DxDoiOrg/101106/YXEA-5MH9-76J5-BACK 2016;35:1435–69. https://doi.org/10.1106/YXEA-5MH9-76J5-BACK.
6. Govignon Q, Bickerton S, Kelly PA. Simulation of the reinforcement compaction and resin flow during the complete resin infusion process. Composites Part A: Applied Science and Manufacturing 2010;41:45–57. https://doi.org/10.1016/J.COMPOSITESA.2009.07.007.
7. Pierce RS, Falzon BG, Thompson MC. A multi-physics process model for simulating the manufacture of resin-infused composite aerostructures. Composites Science and Technology 2017;149:269–79. https://doi.org/10.1016/J.COMPSCITECH.2017.07.003.
8. Acheson JA, Simacek P, Advani SG. The implications of fiber compaction and saturation on fully coupled VARTM simulation. Composites Part A: Applied Science and Manufacturing 2004;35:159–69. https://doi.org/10.1016/J.COMPOSITESA.2003.02.001.
9. Li X, Lua J, Elenchezhian MRP, Enos R, Zhang D. A Multiphysics Coupling of Resin Infusion and Deformation of Fiber Preform Using Customized Star-CCM+ and Abaqus. AIAA Science and Technology Forum and Exposition, AIAA SciTech Forum 2022 2022. https://doi.org/10.2514/6.2022-1419.
10. Chen W, Zhang D. A micromechanics-based processing model for predicting residual stress in fiber-reinforced polymer matrix composites. Composite Structures 2018;204:153–66. https://doi.org/10.1016/J.COMPSTRUCT.2018.07.016.
11. Rusu RB, Cousins S. 3D is here: Point Cloud Library (PCL). Proceedings - IEEE International Conference on Robotics and Automation 2011. https://doi.org/10.1109/ICRA.2011.5980567.
12. Endruweit A, Ermanni P. The in-plane permeability of sheared textiles. Experimental observations and a predictive conversion model. Composites Part A: Applied Science and Manufacturing 2004;35:439–51. https://doi.org/10.1016/J.COMPOSITESA.2003.11.002.
13. Chiu HT, Yu B, Chen SC, Lee LJ. Heat transfer during flow and resin reaction through fiber reinforcement. Chemical Engineering Science 2000;55:3365–76. https://doi.org/10.1016/S0009-2509(00)00004-X.
14. Garschke C, Parlevliet PP, Weimer C, Fox BL. Cure kinetics and viscosity modelling of a high-performance epoxy resin film. Polymer Testing 2013;32:150–7. https://doi.org/10.1016/J.POLYMERTESTING.2012.09.011.
15. Barari B, Simacek P, Yarlagadda S, Crane RM, Advani SG. Prediction of process-induced void formation in anisotropic Fiber-reinforced autoclave composite parts. International Journal of Material Forming 2019 13:1 2019;13:143–58. https://doi.org/10.1007/S12289-019-01477-4.
16. Li Y, Li M, Gu Y, Zhang Z. Numerical and experimental study on the effect of lay-up type and structural elements on thickness uniformity of L-shaped laminates. Applied Composite Materials 2009;16. https://doi.org/10.1007/s10443-009-9080-z.
17. Hubert P, Vaziri R, Poursartip A. A two-dimensional flow model for the process simulation of complex shape composite laminates. International Journal for Numerical Methods in Engineering 1999;44. https://doi.org/10.1002/(SICI)1097-0207(19990110)44:1<1::AID-NME481>3.0.CO;2-K.
18. Geng Y, Jiang J, Chen N. Local impregnation behavior and simulation of non-crimp fabric on curved plates in vacuum assisted resin transfer molding. Composite Structures 2019;208. https://doi.org/10.1016/j.compstruct.2018.10.054.
19. Betteridge BG. LCM Permeability Characterization Over Mold Curvature 2020.